ACS APPLIED MATERIALS & INTERFACES

www.acsami.org

Research Article

Morphology-Graded Silicon Nanowire Arrays via Chemical Etching: Engineering Optical Properties at the Nanoscale and Macroscale

Fedja J. Wendisch, Mehri Abazari, Hossein Mahdavi, Marcel Rey, Nicolas Vogel, Maurizio Musso, Oliver Diwald, and Gilles R. Bourret*

Cite This: *ACS Appl. Mater. Interfaces* 2020, 12, 13140–13147

Read Online

ACCESS | Metrics & More | Article Recommendations | Supporting Information

ABSTRACT: We report on a quick, simple, and cost-effective solution-phase approach to prepare centimeter-sized morphology-graded vertically aligned Si nanowire arrays. Gradients in the nanowire diameter and shape are encoded through the macroscale substrate via a "dip-etching" approach, where the substrate is removed from a KOH etching solution at a constant rate, while morphological control at the nanowire level is achieved via sequential metal-assisted chemical etching and KOH etching steps. This combined approach provides control over light absorption and reflection within the nanowire arrays at both the macroscale and nanoscale, as shown by UV–vis spectroscopy and numerical three-dimensional finite-difference time-domain simulations. Macroscale morphology gradients yield arrays with gradually changing optical properties. Nanoscale morphology control is demonstrated by synthesizing arrays of bisegmented nanowires, where the nanowires are composed of two distinct segments with independently controlled lengths and diameters. Such nanowires are important to tailor light–matter interactions in functional devices, especially by maximizing light absorption at specific wavelengths and locations within the nanowires.

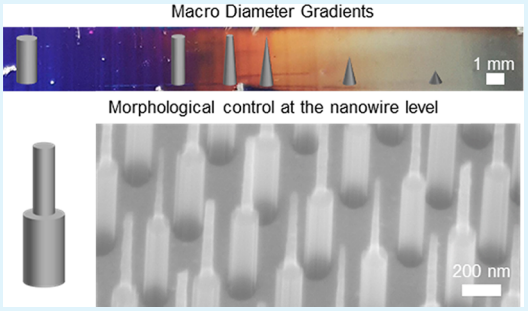

KEYWORDS: *Si nanowire arrays, metal-assisted chemical etching, colloidal lithography, graded substrate, KOH etching, structural colors*

INTRODUCTION

Silicon is an earth-abundant, nontoxic element and has a band gap nearly matching the solar spectrum, which makes it a crucial component for micro- and optoelectronic devices. Nanostructuring silicon into arrays of vertically aligned silicon nanowires (VA-SiNWs) adds significant versatility to this key element: changes in the nanowire length, diameter, and spacing can be used to modulate many of the VA-SiNW properties, such as light absorption and scattering,[1−6] surface electric field enhancement,[7] electron–hole recombination,[8,9] quantum confinement,[10,11] hydrophobicity,[12] mechanical response,[13] biocompatibility,[14−16] or electrocatalyst loading.[17,18] The rich interaction of VA-SiNWs with light,[1−6] which encompasses light trapping, Mie resonances, and waveguiding and diffractive effects, is especially attractive for optical applications such as solar conversion, sensing, or photocatalysis.[3,15−28] In particular, light absorption can be controlled by adjusting nanowire cross-sectional morphology and diameter,[1−3,22,23,29] while reflection can be suppressed using nanostructured "black" silicon, which is critical to improve single-crystalline silicon solar cell conversion efficiency.[30] To date, difficulties in the preparation of VA-SiNW arrays have impeded their widespread use.

Single-crystalline VA-SiNW arrays can be synthesized in the gas phase either via vapor–liquid–solid (VLS) synthesis[31] or reactive ion etching (RIE)[3] and in solution via metal-assisted chemical etching (MACE).[32−35] MACE offers the advantage of being cost-effective, simple, large scale, and widely available to researchers without access to the clean room facilities required for RIE. While VLS synthesis generates impurities that can alter the nanowire electronic properties due to the use of a metal catalyst,[36] nanowires produced via MACE have the pristine composition and crystalline orientation of the parent silicon wafer.[32] The wire spacing and diameter can be routinely controlled in the >400 nm range using standard photolithographic masks. To access dimensions in the sub-400 nm range, electron-beam lithography is required, which is slow and requires specialized equipment. Colloidal lithography is a great alternative to prepare nanostructured masks with dimensions down to approximately 100 nm.[34,37,38] Its combination with MACE yields a simple chemistry-based approach to produce centimeter-scale VA-SiNW arrays with well-defined nanowire lengths, diameters, and spacings.[34,38]

The independent control over nanowire shape, dimension, and composition, while maintaining simple, fast, and large-

Received: November 26, 2019
Accepted: February 21, 2020
Published: March 4, 2020

scale fabrication capabilities, is a major challenge in nanowire synthesis. Exotic structures, such as nanowires with a periodically modulated diameter or with a cone shape, can be prepared with specific RIE processes.[3,22,23] VLS syntheses can be modified to produce nanowires with spatially controlled dopant concentrations (gold impurity or acceptor/donor atoms) along the nanowire length, which, in combination with selective etching, provides an elegant way to control the nanowire diameter in the axial direction.[13,39] Control over the catalyst droplet size under specific conditions has also been demonstrated to tune the nanowire diameter via VLS synthesis.[40] Using MACE, it is possible to synthesize nanowires with cylindrical or hexagonal cross section,[34] as well as nanowires with a zigzag morphology along the wire axis.[41] Even more complex architectures can be synthesized using the three-dimensional electrochemical axial lithography (3DEAL), where a porous membrane is formed around the VA-SiNWs to add metal shells at specific locations via electrochemical deposition and selective etching.[42] These previous studies have shown that morphologically engineered VA-SiNW arrays have enhanced properties, useful for nanowire solar cells,[3,43] photonics,[44] and surface-enhanced Raman spectroscopy (SERS).[42,45,46] Despite these demonstrations, a simple strategy to create tailored morphologies is still missing.

In addition to engineer structure geometry at the single-nanowire level, controlling dimension and shape gradients at the macroscale can provide substrates with continuously changing properties, ideal to fundamentally investigate geometry–function relationships and optimize array geometries for a specific application. VA-SiNW arrays with spacing gradients were recently synthesized using microgel-based colloidal lithography, leading to substrates with a progressive change in reflectance across the UV–vis range.[33] However, a similar concept allowing precise and progressive changes in nanowire morphology across the substrate does not exist to this date. Such substrates would be especially relevant for systems that rely on the tunable optical properties of VA-SiNW arrays, such as color filters,[1,6,27] ultrathin solar cells,[3,19,21] photodetectors,[28] photocatalytic systems,[17,20,24−26] intracellular probes,[15,16] or SERS substrates.[42,45,46]

RESULTS AND DISCUSSION

In this paper, we report on a quick, simple, cost-effective, and solution-phase synthesis combining MACE and wet chemical KOH etching to structure individual nanowires and create defined gradients throughout centimeter-sized substrates (Figure 1). Hexagonal gold nanohole arrays prepared via colloidal lithography (Figure 1a) yield VA-SiNW arrays after MACE (Figure 1b–d). KOH is a well-known silicon etchant, routinely used in microfabrication, which offers a simple route to reduce the diameter of silicon nanowires (Figure 1b).[47] Gradients in the nanowire diameter and shape are encoded through the macroscale substrate via "dip-etching", where the substrate is removed from the etching solution at a constant rate (Figure 1c), and at the nanowire level via sequential MACE and KOH etching steps (Figure 1d). These approaches provide control over light absorption within the VA-SiNW arrays at both the macroscale and nanoscale, as shown by UV–vis spectroscopy and numerical three-dimensional electromagnetic simulations based on the finite-difference time-domain (FDTD) method.

Diameter-Controlled SiNW Arrays. Diameter-controlled SiNW arrays are fabricated as illustrated in Figure 1a,b: VA-

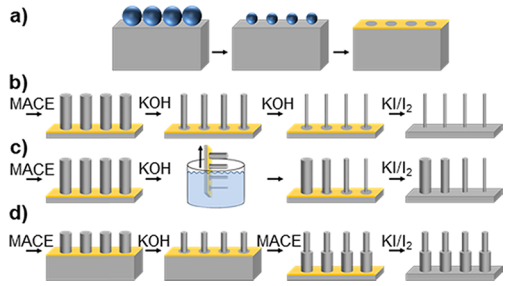

Figure 1. Synthesis scheme of morphology-graded VA-SiNW arrays. (a) Preparation of the nanostructured gold mask via colloidal lithography: self-assembly of spherical colloidal particles (in blue) on a Si wafer (in gray) followed by size reduction to form a nonclose-packed array; deposition of a gold film through the colloidal mask and subsequent liftoff of the templating spheres yield a gold nanohole film array (in yellow). (b–d) First step (left): synthesis of VA-SiNW arrays via MACE. Last step (right): gold film dissolution in KI/I_2 prior to the optical characterization. (b) Control of nanowire diameter: the VA-SiNW array is immersed in KOH etchant for a defined duration. (c) Control of a macroscopic diameter and shape gradient via dip-etching: the VA-SiNW array is removed from the KOH etching solution at a constant rate. (d) Control of nanoscale morphology in bisegmented Si nanowires: sequential MACE and KOH etching steps yield SiNWs composed of segments with tunable lengths and diameters.

SiNW arrays with nominal diameters of 120 and 410 nm and nanowire pitches of ca. 430 and 590 nm, respectively, were synthesized via colloidal lithography and MACE (details in the Supporting Information). Concentrated (20 wt %) or diluted (0.2 wt %) KOH solution homogeneously etches the Si nanowires down to ca. 70% of the original nanowire diameter without significant changes in morphology (Figure 2, Figures S1 and S2, and Table S1). Because KOH etches SiO_2 slower than Si, a small variation in the native SiO_2 thickness after MACE can lead to discrepancy in the Si etch rate. Thus, we recommend to perform KOH etching immediately after an HF pre-etch (i.e., within less than 1 min). VA-SiNWs with diameters in the sub-300 nm range were previously found to sustain leaky waveguide modes in the UV–vis range with characteristic dips in the reflectance spectrum due to increased absorption, which are responsible for their vivid colors.[1,2,4] The number of leaky modes and their resonance wavelength depends on the wire diameter: at diameters $d < 100$ nm, the HE_{11} mode can be sustained, while for $d > 100$ nm, other modes, such as the HE_{12}, emerge at lower wavelengths.[2] These modes red-shift as the diameter increases.[1,2] This can be seen in Figure 2, where the HE_{11} mode is observed at ca. 390, 440, 525, and 585 nm for wires with diameters of 63, 77, 87, and 118 nm, respectively (Figure 2f). The appearance of the HE_{12} mode can be seen at ca. 390 nm for $d = 118$ nm. The relative broadness of the reflectance dips originates from the small pitch of the arrays (~430 nm), which allows the modes to couple due to their large radial extension, leading to a broadening of the absorption.[2] Consequently, arrays with average nanowire diameters of 63, 77, 87, and 118 nm appear gray, yellow, purple, and blue, respectively (Figure 2a–d and Figure S2). This confirms the strong influence of the nanowire diameter on the interaction between VA-SiNW arrays and light.[1,2,4]

Shape and Diameter Gradients. Shape and diameter gradients were encoded within centimeter-sized substrates via dip-etching (Figure 1c): the VA-SiNWs were immersed in a

https://dx.doi.org/10.1021/acsami.9b21466
ACS Appl. Mater. Interfaces 2020, 12, 13140−13147

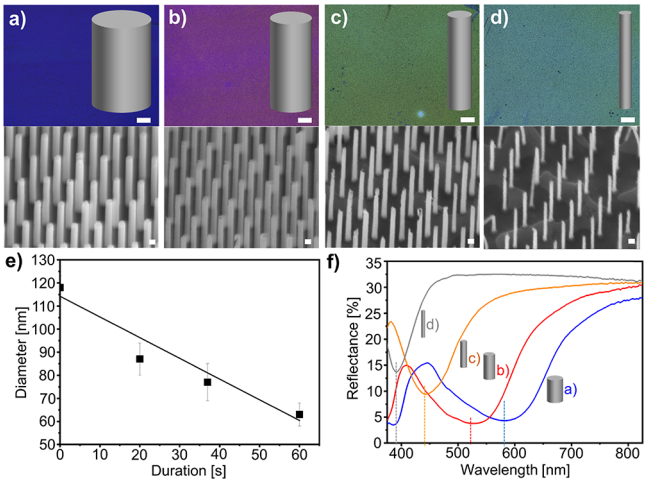

Figure 2. Control of SiNW diameter via KOH etching. (a–d) Top row: optical microscopy images of homogeneously etched silicon nanowire arrays using an aqueous 0.2 wt % KOH solution. Scale bars: 100 μm. Bottom row: secondary electron SEM images. Tilt angle: 30°. Scale bars: 100 nm. (a) Reference substrate after MACE, d = 118 nm. (b) SiNWs with d = 87 nm, after 20 s KOH etching. (c) SiNWs with d = 77 nm, after 40 s KOH etching. (d) SiNWs with d = 63 nm, after 60 s KOH etching. (e) Graph showing the wire diameter as a function of KOH etching duration. Pitch = 430 nm. KOH etching was performed immediately (i.e., within 30 s) after an HF pretreatment. (f) Reflectance spectra of the SiNW arrays shown in a–d. The characteristic minimum in reflection blue-shifts for smaller diameters. Photographs of the substrate and the area used for reflectance measurements can be found in Figure S2.

two-phase mixture composed of an n-hexane phase at the top and an aqueous KOH solution at the bottom. Removal of the Si substrate at a constant rate produces an array composed of SiNWs with graded morphologies (Figure 3). A low KOH concentration (0.2 wt %) and slow removal rate (200 mm/h) were used to prevent the nucleation of large H_2 bubbles that form at the substrate surface due to the reaction between KOH, H_2O, and Si, which can lead to spatial inhomogeneity in the etching rate (Figure S3). The organic phase at the top of the aqueous etching solution limits the amount of residual KOH solution trapped within the nanowires, avoiding etching of the substrate after removal (Figure S3). An HF pre-etch was used to dissolve the native SiO_2 before every dip-etching to improve etching reproducibility (details in the Supporting Information). Both top-view and tilted-view scanning electron microscopy (SEM) was performed every millimeter to analyze the gradual change in the dimension and shape of the VA-SiNWs. As seen in Figure 3c, despite the HF treatment, there is a lag before the wires start to be etched due to the growth of a thin native oxide between MACE and the dip-etching experiment. Additionally, the wires located at the beginning of the gradient, that is, almost unetched by KOH (location in Figure 3e), have a cylindrical morphology with a slight tapering: the diameter at the top of the nanowires is ca. 10% smaller than at the bottom. Within a distance of 10 mm, the nanowire diameter gradually decreases from ca. 110 nm down to 70 nm, while the cylindrical morphology and the 1.7 micrometer length are mostly preserved (Figure 3f). Within the next 5 mm, the nanowire quickly takes a pronounced tapered shape: the top nanowire diameter progressively reduces to ca. 20 nm, at which point the nanowire becomes a nanocone with a ca. 1.2 micrometer length (Figure 3g,h).

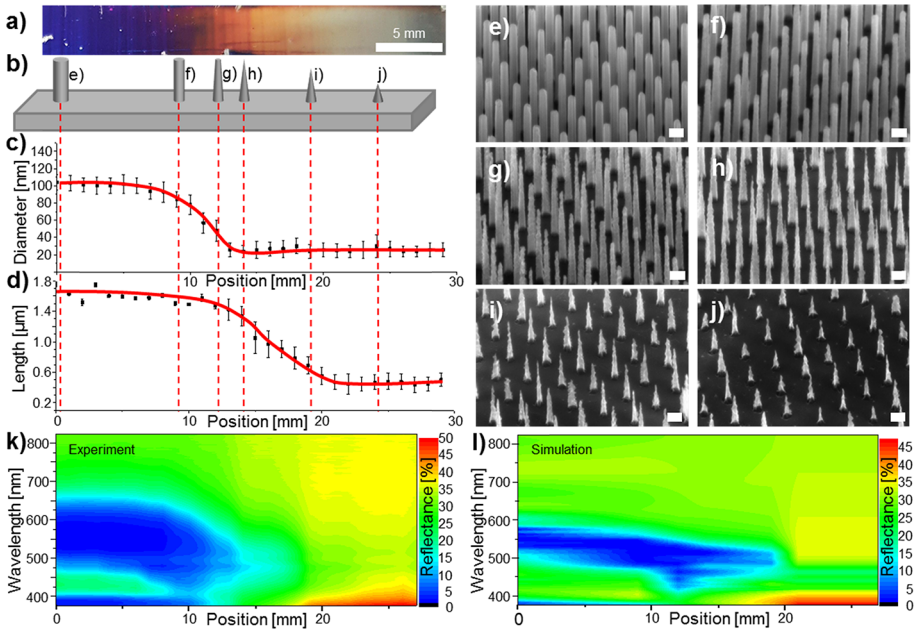

Figure 3. Shape and dimension gradients at the macroscale via dip-etching. (a) Photograph of the centimeter-sized gradient sample showing continuously varying structural colors. (b) Scheme showing the gradual change in the VA-SiNW morphology at different locations on the substrate. (c, d) Evolution of the nanowire morphology across the sample. The nanowire top (c) diameter and (d) length were measured every millimeter. The red lines are a guide to the eye. (e–j) Secondary electron SEM images showing different locations on the substrate. Tilt angle: 45°. Scale bars: 200 nm. (k) Contour map of the experimentally measured reflectance spectra as a function of location. The reflectance was measured every millimeter by using an ~7 mm^2 pinhole. (l) Contour map of the simulated reflectance spectra. The spectra of the six structures shown in e–j were simulated, and the data points in between these locations were extrapolated. The maximum reflectance values were 49.80 and 47.20% for the experimental and the simulated maps, respectively.

https://dx.doi.org/10.1021/acsami.9b21466
ACS Appl. Mater. Interfaces 2020, 12, 13140–13147

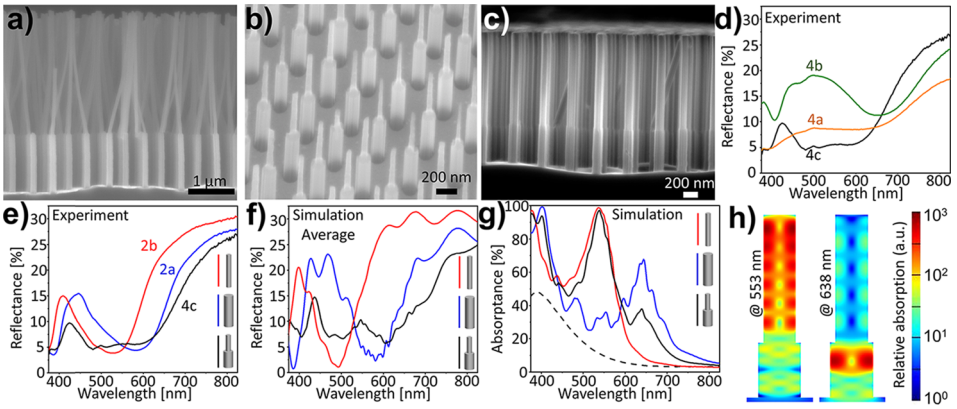

Figure 4. Bisegmented nanowires via sequential MACE and KOH etching. (a–c) Secondary electron SEM images of different bisegmented VA-SiNW arrays. (a) Nanowires composed of a top segment with a high aspect ratio of 38 (d_{top} = 69 nm) and a bottom segment with a low aspect ratio of 9 (d_{bottom} = 137 nm). The difference in aspect ratios leads to a selective bundling of the top part of the wires. (b) d_{top} = 60 nm and d_{bottom} = 143 nm. (c) $d_{exp,top}$ = 98 nm and $d_{exp,bottom}$ = 133 nm. (d) Experimental reflectance spectra of the substrates shown in a–c. (e) Experimental reflectance spectra. Black curve: bisegmented VA-SiNWs shown in c. Red curve: single-diameter VA-SiNWs with d_{exp1} = 87 nm from Figure 2b. Blue curve: single-diameter VA-SiNW with d_{exp2} = 118 nm from Figure 2a. (f) Simulated reflectance spectra of arrays with similar dimensions as those used in e, same color code. The spectra were obtained by averaging the spectra over different diameters to take into account the wire size distribution (Table S5 for more details). (g) Simulated absorptance spectra of VA-SiNW arrays with different diameters but with the same volume, set by their length, to allow direct comparison of the simulated optical data, and highlighting the opportunity to control light absorption by engineering nanowires composed of segments with different dimensions. Black curve: $d_{sim,top}$ = 100 nm, $d_{sim,bottom}$ = 130 nm. Red curve: d_{sim1} = 100 nm. Blue curve, d_{sim2} = 130 nm. The corresponding simulated reflectance and transmittance spectra are shown in Figure S9. The dashed black line corresponds to flat silicon. (h) Two-dimensional maps of the simulated relative absorption within the bisegmented nanowires simulated in g at 553 and 638 nm.

This shows that KOH etching proceeds via a preferential etching of the top of the wires, more exposed to the etching solution, which thus dissolves faster. In the final etching stages, corresponding to the next 10 mm, the nanocone length progressively decreases down to ca. 400 nm (Figure 3i,j). Diffuse reflectance measurements performed every millimeter show a progressive change that expectedly follows the changes in nanowire dimensions and shapes (Figure 3k, Figure S4, and Tables S1 and S3). The broad reflectance dip centered at around ca. 560 nm blue-shifts to ca. 475 nm as the wire diameter decreases (locations corresponding to Figure 3e–h). Tapered and conical shapes are known to produce broader resonances,[48] which, in addition to the relatively short array pitch,[2] could explain the broadness of the reflectance dip measured. Such structures are technologically interesting for their light trapping properties (Table S3) and have been previously used as antireflection coatings for photovoltaics.[22,23] As the nanocone length progressively decreases, an increase in reflectance is observed: the lower amount of nanostructured silicon present leads to a lower absorption (locations corresponding to Figure 3h–j). The FDTD method was used to simulate the reflectance spectra of the periodic VA-SiNW arrays with the same shapes and dimensions as the experimental samples shown in Figure 3e–j. The simulated spectra qualitatively reproduce all essential features of the experimental data with varying shapes and dimensions (Figure 3k,l and Figure S4). The experimental spectra show broader features compared to the numerical simulations, which we attribute to the distribution in diameter, shape, and length of the nanowires sampled within the ~7 mm^2 area used for the reflectance measurements (see Table S1 for dimensions). We demonstrate control over the gradient profile by adjusting the removal rate: at a removal rate of 200 mm/h, the nanowire diameter decreases linearly by ca. 9.5 nm/mm (Figure 3 and Figure S3), while at a removal rate of 4000 mm/h, the nanowire diameter changes more gradually across the sample at ca. 1.3 nm/mm (Figure S5). Overall, these results show that dip-etching provides a tunable, uniform, and continuous etching of the nanostructured Si substrates, leading to concomitant changes in diameter, length, and shape. However, to date, the approach cannot be used to independently modify each of these parameters, although this might be possible in the future by optimizing the etching conditions.

Asymmetric Bisegmented VA-SiNWs. Asymmetric bisegmented VA-SiNWs composed of tunable segments with different diameters and lengths were synthesized using the following etching sequence: MACE, KOH etching, and MACE (Figure 1d, Figure 4, and Table S2). The first segment length is controlled by the first MACE duration, while its diameter depends on the KOH etching duration. Interestingly, the gold film present at the bottom of the VA-SiNWs after MACE does not delaminate and is very stable during KOH etching, as shown via SEM analysis (Figure S6). This allows the second MACE step to proceed properly, forming a second segment with a diameter equal to the diameter of the gold nanohole array prepared from the colloidal mask. This simple approach can be used to modulate the nanowire diameter along the wire axis. It is possible to synthesize wires where the top segment aspect ratio is high enough to induce bundling via drying-induced capillary forces, while the bottom segment remains vertical (Figure 4a, to compare with Figure 4b,c). Thus, sequential MACE and KOH etching can be used to control nanowire aggregation in three dimensions, which provides an additional degree of freedom to engineer hierarchical system configurations.[49,50] The effect of bundling on the array optical properties is shown on Figure 4d: bundled arrays with d_{top} = 69 nm and d_{bottom} = 137 nm (orange curve, SEM image shown in Figure 4a) have a much lower and broader reflectance over the visible range than shorter and straight wires with d_{top} = 60 nm and d_{bottom} = 143 nm (green curve, SEM image shown in

https://dx.doi.org/10.1021/acsami.9b21466
ACS Appl. Mater. Interfaces 2020, 12, 13140–13147

Figure 4b), which have two well-defined reflectance dips at ca. 410 and 680 nm.

Since light absorption strongly depends on the nanowire diameter (Figure 2),[1−4] the ability to engineer multiple diameters within an individual nanowire provides an additional opportunity to tune optical properties. Figure 4c shows an array of bisegmented VA-SiNWs with top and bottom segment diameters of $d_{exp,top}$ = 98 nm and $d_{exp,bottom}$ = 133 nm and lengths of $l_{exp,top}$ ≈ 1340 nm and $l_{exp,bottom}$ ≈ 590 nm, respectively. The reflectance spectrum of this bisegmented VA-SiNW array, shown in Figure 4e (black curve), has a much wider dip than the one measured for the two corresponding single-diameter nanowire arrays (d_{exp1} = 87 nm, red curve and d_{exp2} = 118 nm, blue curve). Because the three VA-SiNW samples have different nanowire lengths and volumes (see Table S4 for the array dimensions), comparing the absolute values at the reflectance minima is not straightforward. The reflectance dips, however, can be compared because they only depend on the wire diameter (Figure S7). In the simulated reflectance spectra of bisegmented VA-SiNW arrays with similar dimensions, we observe a broadening of the reflectance minimum (Figure S8). Closely spaced oscillations are seen in the simulated spectra of the VA-SiNW arrays at wavelengths >450 nm where silicon does not absorb significantly. These oscillations are due to Fabry−Pérot resonances: light reflection at the top and bottom of the nanowire array can lead to constructive and destructive interferences at specific wavelengths. As expected, these Fabry−Pérot interferences depend on film thickness (i.e., nanowire length, see Figure S7).[4,33,48] They are not observed in the experimental reflectance spectra, most likely because of the array size distribution over the area probed during the UV−vis measurement. To match the experimental spectra of Figure 4e, we simulated the same arrays (i.e., the same wire pitch and wire length as the corresponding synthesized structures) with eight different wire diameters (see Table S5 for dimensions; more details in the simulation section of the Supporting Information). A weighted average based on the size distribution measured via SEM gives a better agreement with the experiments (Figure 4f): the reflectance values and location of the dips are well reproduced. The broadening of the reflectance dip is also observed for the simulated bisegmented nanowire array. This suggests that the lack of fine features observed in the experimental reflectance spectra originates from a distribution in the VA-SiNW array geometrical parameters at the millimeter scale.

To study the beneficial effect of the bisegmented nanowires, we simulated the absorptance spectra of nanowires with different diameters but with the same volume, set by their length, to allow direct comparison of the simulated optical data (Figure 4g and Figure S9, see Table S6 for dimensions). The simulated absorptance spectra show defined maxima at 537 and 642 nm for the reference single-diameter nanowire arrays with d_{sim1} = 100 nm and d_{sim2} = 130 nm, respectively (Figure 4g). As expected, the corresponding bisegmented nanowire array acts as a combination of both nanowire diameters and shows two well-defined absorptance maxima at 553 and 638 nm. Compared to the same volume of planar bulk Si, our simulations show that the single-diameter nanowires provide an overall absorption enhancement of ∼270% over wavelengths in the 375−825 nm range, while the corresponding bisegmented nanowire arrays provide an enhancement of ∼300%. At around 553 nm, the light is mostly absorbed in the top segment, while around 638 nm, the light is mostly absorbed in the bottom segment (Figure 4h). Thus, such nanowires could be used for improved solar conversion and photodetection systems, similar to previous experimental and theoretical reports on similar structures.[3,43]

A tailored design of bisegmented VA-SiNW arrays allows an even better spatial control of light absorption within the nanowires. Bisegmented nanowires with top and bottom diameters of 60 and 140 nm, respectively, such as the ones synthesized and shown in Figure 4b, are expected to have distinct spatial photoresponses under 418 and 736 nm excitations. At 418 nm, the top segment generates ∼10−100 times more charge carriers than the bottom segment, while at 736 nm, the bottom segment generates ∼100 times more charge carriers than the top segment (Figure S10). These large spatial variations in charge carrier photogeneration rates are due to the waveguiding abilities of VA-SiNWs (which are diameter-dependent) and the increased absorption in bulk silicon at shorter wavelengths (Figure 4g, dashed black line). Such asymmetric nanowires could be used for spatioselective photoactivation, where parts of the wires are activated with a given wavelength. The deposition of metal catalysts in these specific regions (via 3DEAL for example)[42] could be especially effective at designing tandem catalytic systems[51−53] where the flux and energy of the incident photons are adjusted to control product selectivity.

CONCLUSIONS

To conclude, we report the use of simple wet chemical etching approaches to shape VA-SiNW arrays at both the macroscale and nanoscale over centimeter-sized substrates. The reported dip-etching technique enables engineering gradual changes in nanostructure geometry and optical properties with high precision. It is quick, simple, and applicable to a wide variety of nanostructured substrates such as metal nanoparticle arrays or other semiconductor nanowire arrays, provided that they can be chemically etched in solution. The sequential use of MACE and KOH etching provides a powerful tool to generate bisegmented nanowire arrays with an independent control of the lengths and diameters of both segments. We demonstrate that such bisegmented nanowire arrays exhibit enhanced and tunable optical properties with the ability to spatially control light absorption within a single nanowire. Since other semiconductors such as GaAs and InP can be nanostructured via MACE, we expect both approaches to enable a facile approach for the design of enhanced nanowire architectures in technologically important III−V semiconductors.[54,55]

EXPERIMENTAL METHODS

Silicon nanowire arrays were synthesized via colloidal lithography and metal-assisted chemical etching (MACE), as previously done by our group.[34,42] Details can be found in the Supporting Information.

Chemical Dissolution of VA-SiNW in KOH Etching Solution. Prior to KOH etching, the sample was immersed in 20 mL of Milli-Q water and 4 mL of hydrofluoric acid to remove the native SiO_2. The substrates were then rinsed three times with Milli-Q water and once with ethanol and immediately etched with KOH (i.e., within 30 s). The gold film present at the bottom of the VA-SiNW was not removed. The substrates were placed on a homemade 3D printed polymer sample holder and immersed in 50 mL of 20 or 0.2 wt % aqueous KOH etching solution. The solution was not prepared fresh but was replaced for each sample. The etching duration depends on the desired diameter (Figure 2e). After etching, the substrate was immediately transferred into a beaker with 1 L of deionized water and finally dried in air.

https://dx.doi.org/10.1021/acsami.9b21466
ACS Appl. Mater. Interfaces 2020, 12, 13140−13147

Synthesis of a Diameter Gradient on the Macroscale via Dip-Etching. Prior to dip-etching, the sample was immersed in 20 mL of Milli-Q water and 4 mL of hydrofluoric acid to remove the native SiO_2. The substrates were then rinsed three times with Milli-Q water and once with ethanol and immediately etched with KOH (i.e., within less than 20 min). The gold film present at the bottom of the VA-SiNW was not removed. Dip-etching was performed using a 0.2 wt % aqueous KOH etching solution. *N*-hexane was poured on top to avoid further etching of the sample after removal from the etching solution. The sample was fixed onto a linear motion driver and pulled out of the etching solution with a constant rate of 200 mm/h (Figure 3 and Figure S3) or 4000 mm/h (Figure S4). Afterward, the sample was rinsed with ethanol and dried in air.

Morphological Control at the Nanowire Level with Sequential MACE and KOH Etching Steps. Diameter gradients at the nanowire level were synthesized using the following etching sequence: MACE, KOH etching, and MACE. The MACE steps were performed as described in the Supporting Information. Durations of MACE were 2 × 2.5 min or 2 × 5 min, depending on the desired VA-SiNW length. For KOH etching, a 5 or 10 wt % KOH solution was utilized for 5−30 s, depending on the desired diameter of the top segment. After each etching step (MACE and KOH), the substrates were cleaned in 20 mL of Milli-Q water and 4 mL of hydrofluoric acid. After MACE or HF, the substrates were rinsed three times with Milli-Q water and once with ethanol and finally dried in air. After KOH etching, the samples were rinsed once in Milli-Q water and dried in air.

■ ASSOCIATED CONTENT

Supporting Information

The Supporting Information is available free of charge at https://pubs.acs.org/doi/10.1021/acsami.9b21466.

Materials and methods, tables listing the dimensions of the VA-SiNW arrays, additional FDTD simulation results (individual reflectance spectra and maps), and additional SEM images (PDF)

■ AUTHOR INFORMATION

Corresponding Author

Gilles R. Bourret − *Department of Chemistry and Physics of Materials, University of Salzburg, A-5020 Salzburg, Austria;* orcid.org/0000-0002-9774-1686; Email: gilles.bourret@sbg.ac.at

Authors

Fedja J. Wendisch − *Department of Chemistry and Physics of Materials, University of Salzburg, A-5020 Salzburg, Austria*

Mehri Abazari − *Department of Chemistry and Physics of Materials, University of Salzburg, A-5020 Salzburg, Austria; School of Chemistry, College of Science, University of Tehran, 14155-6455 Tehran, Iran*

Hossein Mahdavi − *School of Chemistry, College of Science, University of Tehran, 14155-6455 Tehran, Iran*

Marcel Rey − *Institute of Particle Technology, Friedrich-Alexander University Erlangen-Nürnberg, 91058 Erlangen, Germany*

Nicolas Vogel − *Institute of Particle Technology, Friedrich-Alexander University Erlangen-Nürnberg, 91058 Erlangen, Germany;* orcid.org/0000-0002-9831-6905

Maurizio Musso − *Department of Chemistry and Physics of Materials, University of Salzburg, A-5020 Salzburg, Austria;* orcid.org/0000-0001-6631-5206

Oliver Diwald − *Department of Chemistry and Physics of Materials, University of Salzburg, A-5020 Salzburg, Austria;* orcid.org/0000-0002-2425-5281

Complete contact information is available at: https://pubs.acs.org/10.1021/acsami.9b21466

Author Contributions

The manuscript was written through contributions of all authors. All authors have given approval to the final version of the manuscript.

Funding

O.D., G.R.B., and F.J.W. gratefully acknowledge support from the Austrian Science Fund (FWF) for projects P-28797 and P-33159 and the Allergy-Cancer-BioNano (ACBN) research initiative from the University of Salzburg. M.M., G.R.B., and F.J.W. gratefully acknowledge financial support provided by the European Regional Development Fund and Interreg V-A Italy−Austria 2014−2020 through the Interreg Italy−Austria project ITAT 1023 InCIMA http://www.elettra.eu/Prj/InCIMa/. M.R. and N.V. acknowledge support by the Deutsche Forschungsgemeinschaft (DFG) under grant number VO1824/6-1. N.V. also acknowledges support by the Interdisciplinary Center for Functional Particle Systems (FPS).

Notes

The authors declare no competing financial interest.

■ ACKNOWLEDGMENTS

We thank Grant Osborne for his help with the 3D printer to prepare the sample holders used for MACE.

■ ABBREVIATIONS

d, diameter
3DEAL, three-dimensional electrochemical axial lithography
FDTD, finite-difference time-domain
G, relative charge carrier photogeneration rate
MACE, metal-assisted chemical etching
RIE, reactive ion etching
SEM, scanning electron microscopy
SERS, surface-enhanced Raman spectroscopy
VA-SiNW, vertically aligned Si nanowire
VLS, vapor−liquid−solid

■ REFERENCES

(1) Seo, K.; Wober, M.; Steinvurzel, P.; Schonbrun, E.; Dan, Y.; Ellenbogen, T.; Crozier, K. B. Multicolored Vertical Silicon Nanowires. *Nano Lett.* **2011**, *11*, 1851−1856.

(2) Wang, B.; Leu, P. W. Tunable and Selective Resonant Absorption in Vertical Nanowires. *Opt. Lett.* **2012**, *37*, 3756−3758.

(3) Ko, M.; Baek, S. H.; Song, B.; Kang, J. W.; Kim, S. A.; Cho, C. H. Periodically Diameter-Modulated Semiconductor Nanowires for Enhanced Optical Absorption. *Adv. Mater.* **2016**, *28*, 2504−2510.

(4) Fountaine, K. T.; Whitney, W. S.; Atwater, H. A. Resonant Absorption in Semiconductor Nanowires and Nanowire arrays: Relating Leaky Waveguide Modes to Bloch Photonic Crystal Modes. *J. Appl. Phys.* **2014**, *116*, 153106.

(5) Abujetas, D. R.; Paniagua-Domínguez, R.; Sánchez-Gil, J. A. Unraveling the Janus Role of Mie Resonances and Leaky/Guided Modes in Semiconductor Nanowire Absorption for Enhanced Light Harvesting. *ACS Photonics* **2015**, *2*, 921−929.

(6) Proust, J.; Bedu, F.; Gallas, B.; Ozerov, I.; Bonod, N. All-Dielectric Colored Metasurfaces with Silicon Mie Resonators. *ACS Nano* **2016**, *10*, 7761−7767.

(7) Coldarola, M.; Albella, P.; Cortés, E.; Rahmani, M.; Roschuk, T.; Grinblat, G.; Oulton, R. F.; Bragas, A. V.; Maier, S. A. Non-Plasmonic Nanoantennas for Surface Enhanced Spectroscopies with Ultra-Low Heat Conversion. *Nat. Commun.* **2015**, *6*, 7915.

(8) Hagedorn, K.; Forgacs, C.; Collins, S.; Maldonado, S. Design Considerations for Nanowire Heterojunctions in Solar Energy Conversion/Storage Applications. *J. Phys. Chem. C* **2010**, *114*, 12010−12017.
(9) Foley, J. M.; Price, M. J.; Feldblyum, J. I.; Maldonado, S. Analysis of the Operation of Thin Nanowire Photoelectrodes for Solar Energy Conversion. *Energy Environ. Sci.* **2012**, *5*, 5203−5220.
(10) Trivedi, K.; Yuk, H.; Floresca, H. C.; Kim, M. J.; Hu, W. Quantum Confinement Induced Performance Enhancement in Sub-5-nm Lithographic Si Nanowire Transistors. *Nano Lett.* **2011**, *11*, 1412−1417.
(11) Zhao, X.; Wei, C. M.; Yang, L.; Chou, M. Y. Quantum Confinement and Electronic Properties of Silicon Nanowires. *Phys. Rev. Lett.* **2004**, *92*, 236805.
(12) Verplanck, N.; Galopin, E.; Camart, J.-C.; Thomy, V.; Coffinier, Y.; Boukherroub, R. Reversible Electrowetting on Superhydrophobic Silicon Nanowires. *Nano Lett.* **2007**, *7*, 813−817.
(13) Luo, Z.; Jiang, Y.; Myers, B. D.; Isheim, D.; Wu, J.; Zimmerman, J. F.; Wang, Z.; Li, Q.; Wang, Y.; Chen, X.; Dravid, V. P.; Seidman, D. N.; Tian, B. Atomic Gold-Enabled Three-Dimensional Lithography for Silicon Mesostructures. *Science* **2015**, *348*, 1451−1455.
(14) Kim, W.; Ng, J. K.; Kunitake, M. E.; Conklin, B. R.; Yang, P. Interfacing Silicon Nanowires with Mammalian Cells. *J. Am. Chem. Soc.* **2007**, *129*, 7228−7229.
(15) Jiang, Y.; Tian, B. Inorganic Semiconductor Biointerfaces. *Nat. Rev. Mater.* **2018**, *3*, 473−490.
(16) Jiang, Y.; Li, X.; Liu, B.; Yi, J.; Fang, Y.; Shi, F.; Gao, X.; Sudzilovsky, E.; Parameswaran, R.; Koehler, K.; Nair, V.; Yue, J.; Guo, K.; Fang, Y.; Tsai, H.-M.; Freyermuth, G.; Wong, R. C. S.; Kao, C.-M.; Chen, C.-T.; Nicholls, A. W.; Wu, X.; Shepherd, G. M. G.; Tian, B. Rational Design of Silicon Structures for Optically Controlled Multiscale Biointerfaces. *Nat. Biomed. Eng.* **2018**, *2*, 508−521.
(17) Oh, I.; Kye, J.; Hwang, S. Enhanced Photoelectrochemical Hydrogen Production from Silicon Nanowire Array Photocathode. *Nano Lett.* **2012**, *12*, 298.
(18) Su, Y.; Liu, C.; Brittman, S.; Tang, J.; Fu, A.; Kornienko, N.; Kong, Q.; Yang, P. Single-Nanowire Photoelectrochemistry. *Nat. Nanotechnol.* **2016**, *11*, 609−612.
(19) Liu, D.; Yang, D.; Gao, Y.; Ma, J.; Long, R.; Wang, C.; Xiong, Y. Flexible Near-Infrared Photovoltaic Devices Based on Plasmonic Hot-Electron Injection into Silicon Nanowire Arrays. *Angew. Chem., Int. Ed.* **2016**, *55*, 4577−4581.
(20) Mayer, M. T.; Du, C.; Wang, D. Hematite/Si Nanowire Dual-Absorber System for Photoelectrochemical Water Splitting at Low Applied Potentials. *J. Am. Chem. Soc.* **2012**, *134*, 12406−12409.
(21) Garnett, E.; Yang, P. Light Trapping in Silicon Nanowire Solar Cells. *Nano Lett.* **2010**, *10*, 1082−1087.
(22) Jeong, S.; Garnett, E. C.; Wang, S.; Yu, Z.; Fan, S.; Brongersma, M. L.; McGehee, M. D.; Cui, Y. Hybrid Silicon Nanocone−Polymer Solar Cells. *Nano Lett.* **2012**, *12*, 2971−2976.
(23) Jeong, S.; McGehee, M. D.; Cui, Y. All-Back-Contact Ultra-Thin Silicon Nanocone Solar Cells with 13.7% Power Conversion Efficiency. *Nat. Commun.* **2013**, *4*, 2950.
(24) Liu, C.; Tang, J.; Chen, H. M.; Liu, B.; Yang, P. A Fully Integrated Nanosystem of Semiconductor Nanowires for Direct Solar Water Splitting. *Nano Lett.* **2013**, *13*, 2989−2992.
(25) O'Brien, P. G.; Sandhel, A.; Wood, T. E.; Jelle, A. A.; Hoch, L. B.; Perovic, D. D.; Mims, C. A.; Ozin, G. A. Photomethanation of Gaseous CO_2 over Ru/Silicon Nanowire Catalysts with Visible and Near-Infrared Photons. *Adv. Sci.* **2014**, *1*, 1400001.
(26) Agarwal, D.; Aspetti, C. O.; Cargnello, M.; Ren, M.; Yoo, J.; Murray, C. B.; Agarwal, R. Engineering Localized Surface Plasmon Interactions in Gold by Silicon Nanowire for Enhanced Heating and Photocatalysis. *Nano Lett.* **2017**, *17*, 1839−1845.
(27) Khorasaninejad, M.; Abedzadeh, N.; Walia, J.; Patchett, S.; Saini, S. S. Color Matrix Refractive Index Sensors Using Coupled Vertical Silicon Nanowire Arrays. *Nano Lett.* **2012**, *12*, 4228−4234.
(28) Um, H.-D.; Solanki, A.; Jayaraman, A.; Gordon, R. G.; Habbal, F. Electrostatically Doped Silicon Nanowire Arrays for Multispectral Photodetectors. *ACS Nano* **2019**, *13*, 11717−11725.
(29) Kim, S.-K.; Day, R. W.; Cahoon, J. F.; Kempa, T. J.; Song, K.-D.; Park, H.-G.; Lieber, C. M. Tuning Light Absorption in Core/Shell Silicon Nanowire Photovoltaic Devices through Morphological Design. *Nano Lett.* **2012**, *12*, 4971−4976.
(30) Savin, H.; Repo, P.; von Gastrow, G.; Ortega, P.; Calle, E.; Garín, M.; Alcubilla, R. Black Silicon Solar Cells with Interdigitated Back-Contacts Achieve 22.1% Efficiency. *Nat. Nanotechnol.* **2015**, *10*, 624−628.
(31) Morales, A. M.; Lieber, C. M. A Laser Ablation Method for the Synthesis of Crystalline Semiconductor Nanowires. *Science* **1998**, *279*, 208−211.
(32) Huang, Z.; Geyer, N.; Werner, P.; de Boor, J.; Gösele, U. Metal-Assisted Chemical Etching of Silicon: a Review. *Adv. Mater.* **2011**, *23*, 285−308.
(33) Rey, B. M.; Elnathan, R.; Ditcovski, R.; Geisel, K.; Zanini, M.; Fernandez-Rodriguez, M.-A.; Naik, V. V.; Frutiger, A.; Richtering, W.; Ellenbogen, T.; Voelcker, N. H.; Isa, L. Fully Tunable Silicon Nanowire Arrays Fabricated by Soft Nanoparticle Templating. *Nano Lett.* **2016**, *16*, 157−163.
(34) Wendisch, F. J.; Oberreiter, R.; Salihovic, M.; Elsaesser, M. S.; Bourret, G. R. Confined Etching within 2D and 3D Colloidal Crystals for Tunable Nanostructured Templates: Local Environment Matters. *ACS Appl. Mater. Interfaces* **2017**, *9*, 3931−3939.
(35) Tieu, T.; Alba, M.; Elnathan, R.; Cifuentes-Rius, A.; Voelcker, N. H. Advances in Porous Silicon−Based Nanomaterials for Diagnostic and Therapeutic Applications. *Adv. Therap.* **2019**, *2*, 1800095.
(36) Chen, W.; Yu, L.; Misra, S.; Fan, Z.; Pareige, P.; Patriarche, G.; Bouchoule, S.; Cabarrocas, P. R. i. Incorporation and Redistribution of Impurities into Silicon Nanowires During Metal-Particle-Assisted Growth. *Nat. Commun.* **2014**, *5*, 4134.
(37) Vogel, N.; Weiss, C. K.; Landfester, K. From Soft to Hard: the Generation of Functional and Complex Colloidal Monolayers for Nanolithography. *Soft Matter* **2012**, *8*, 4044−4061.
(38) Tang, J. S. J.; Bader, R. S.; Goerlitzer, E. S. A.; Wendisch, J. F.; Bourret, G. R.; Rey, M.; Vogel, N. Surface patterning with SiO_2@PNiPAm core-shell particles. *ACS Omega* **2018**, *3*, 12089−12098.
(39) Christesen, J. D.; Pinion, C. W.; Grumstrup, E. M.; Papanikolas, J. M.; Cahoon, J. F. Synthetically Encoding 10 nm Morphology in Silicon Nanowires. *Nano Lett.* **2013**, *13*, 6281−6286.
(40) Kim, W.; Dubrovskii, V. G.; Vukajlovic-Plestina, J.; Tütüncüoglu, G.; Francaviglia, L.; Güniat, L.; Potts, H.; Friedl, M.; Leran, J.-B.; Fontcuberta i Morral, A. Bistability of Contact Angle and Its Role in Achieving Quantum-Thin Self-Assisted GaAs nanowires. *Nano Lett.* **2018**, *18*, 49−57.
(41) Chen, Y.; Li, L.; Zhang, C.; Tuan, C.-C.; Chen, X.; Gao, J.; Wong, C.-P. Controlling Kink Geometry in Nanowires Fabricated by Alternating Metal-Assisted Chemical Etching. *Nano Lett.* **2017**, *17*, 1014−1019.
(42) Wendisch, F. J.; Saller, M. S.; Eadie, A.; Reyer, A.; Musso, M.; Rey, M.; Vogel, N.; Diwald, O.; Bourret, G. R. Three-Dimensional Electrochemical Axial Lithography on Si Micro- and Nanowire Arrays. *Nano Lett.* **2018**, *18*, 7343−7349.
(43) Fan, Z.; Kapadia, R.; Leu, P. W.; Zhang, X.; Chueh, Y.-L.; Takei, K.; Yu, K.; Jamshidi, A.; Rathore, A. A.; Ruebusch, D. J.; Wu, M.; Javey, A. Ordered Arrays of Dual-Diameter Nanopillars for Maximized Optical Absorption. *Nano Lett.* **2010**, *10*, 3823−3827.
(44) Kim, S.; Kim, K.-H.; Hill, D. J.; Park, H.-G.; Cahoon, J. F. Mie-Coupled Bound Guided States in Nanowire Geometric Superlattices. *Nat. Commun.* **2018**, *9*, 2781.
(45) Wells, S. M.; Merkulov, I. A.; Kravchenko, I. I.; Lavrik, N. V.; Sepaniak, M. J. Silicon Nanopillars for Field-Enhanced Surface Spectroscopy. *ACS Nano* **2012**, *6*, 2948−2959.
(46) Lin, D.; Wu, Z.; Li, S.; Zhao, W.; Ma, C.; Wang, J.; Jiang, Z.; Zhong, Z.; Zheng, Y.; Yang, X. Large-Area Au-Nanoparticle-

https://dx.doi.org/10.1021/acsami.9b21466
ACS Appl. Mater. Interfaces 2020, 12, 13140−13147

Functionalized Si Nanorod Arrays for Spatially Uniform Surface-Enhanced Raman Spectroscopy. *ACS Nano* **2017**, *11*, 1478−1487.
(47) Hsu, H.-F.; Wang, J.-Y.; Wu, Y.-H. KOH Etching for Tuning Diameter of Si Nanowire Arrays and Their Field Emission Characteristics. *J. Electrochem. Soc.* **2014**, *161*, H53−H56.
(48) Solanki, A.; Crozier, K. Vertical Germanium Nanowires as Spectrally-Selective Absorbers Across the Visible-to-Infrared. *Appl. Phys. Lett.* **2014**, *105*, 191115.
(49) Sidorenko, A.; Krupenkin, T.; Taylor, A.; Fratzl, P.; Aizenberg, J. Reversible Switching of Hydrogel-Actuated Nanostructures into Complex Micropatterns. *Science* **2007**, *315*, 487−490.
(50) Duan, H.; Berggren, K. K. Directed Self-Assembly at the 10 nm Scale by Using Capillary Force-Induced Nanocohesion. *Nano Lett.* **2010**, *10*, 3710−3716.
(51) Morales-Guio, C. G.; Cave, E. R.; Nitopi, S. A.; Feaster, J. T.; Wang, L.; Kuhl, K. P.; Jackson, A.; Johnson, N. C.; Abram, D. N.; Hatsukade, T.; Hahn, C.; Jaramillo, T. F. Improved CO_2 Reduction Activity towards C_{2+} Alcohols on a Tandem Gold on Copper Electrocatalyst. *Nat. Catal.* **2018**, *1*, 764−771.
(52) Lohr, T. L.; Marks, T. J. Orthogonal Tandem Catalysis. *Nat. Chem.* **2015**, *7*, 477.
(53) Xie, C.; Chen, C.; Yu, Y.; Su, J.; Li, Y.; Somorjai, G. A.; Yang, P. Tandem Catalysis for CO_2 Hydrogenation to C_2−C_4 Hydrocarbons. *Nano Lett.* **2017**, *17*, 3798−3802.
(54) DeJarld, M.; Shin, J. C.; Chern, W.; Chanda, D.; Balasundaram, K.; Rogers, J. A.; Li, X. Formation of High Aspect Ratio GaAs Nanostructures with Metal-Assisted Chemical Etching. *Nano Lett.* **2011**, *11*, 5259−5263.
(55) Kim, S. H.; Mohseni, P. K.; Song, Y.; Ishihara, T.; Li, X. Inverse Metal-Assisted Chemical Etching Produces Smooth High Aspect Ratio InP Nanostructures. *Nano Lett.* **2015**, *15*, 641−648.

https://dx.doi.org/10.1021/acsami.9b21466
ACS Appl. Mater. Interfaces 2020, 12, 13140−13147